Optical and structural properties of PbS:Bi^{3+} nanocrystals

R. Gutiérrez Pérez[a], O. Portillo Moreno[a,*], L. Chaltel Lima[a], M. Chávez Portillo[b],
R. Palomino Merino[c], and M. Zamora Totozintle[a]
[a]*Materials Science Laboratory, Facultad de Ciencias Químicas, Universidad Autónoma de Puebla, P.O. Box 1067, Puebla, Pue., 72001 México.*
[*]*Tel. (01 222) 2-29-55-00 Ext. 7519.*
e-mail: osporti@yahoo.com.mx
[b]*Universidad Autónoma de Puebla, Puebla, Pue., 72001 México.*
[c]*Facultad de Ciencias Fisicomatemáticas, Posgrado en Optoelectrónica de la Benemérita Universidad Autónoma de Puebla, Puebla, P.O. Box 1067, C.P. 72001, México,*

Received 22 April 2015; accepted 15 June 2015

We report here the growth of nanocrystalline PbS thin films by chemical bath and the effects of doping on the structural and electronics properties as a function of Bi^{3+} concentration. Doping of such PbS films with Bi^{3+} produces considerable optical and structural changes that have an effect on the material properties. The morphological changes of the layers were followed by Atomic Force Microscopy (AFM) and Scanning Electron Microscopy (SEM). X-ray diffraction (XRD) spectra show growth of the zinc blende phase. The grain size for the undoped samples was found to be $\sim$ 32 nm, whereas that for the doped samples was 25-15 nm, thus confirming AFM and SEM results. A conspicuous shift for the forbidden band gap energy was observed by optical absorption from 1.2 eV for the undoped samples to a 1.7-2.0 eV range for the doped films.

Keywords: Chemical bath; grain size; cell potential; nanoparticles; coordination complex; doping.

PACS: 71.20.Nr; 68.55.A; 64.70.kg

1. Introduction

In recent years there has been an increasing interest in the synthesis of nanomaterials due to their outstanding physical and chemical properties and their potential applications. Following the pioneer theoretical study of semiconductor nanocrystals (NCs) by Brus [1], tremendous efforts have been made to synthetize NCs with quantum size effects [2] and it has been proposed that, because of their optical and electrical properties, these semiconductor NCs are likely to play a key role in optoelectronic applications including chemical sensing devices [3]. Quantum size effects are usually found in nanocrystallites measuring less than 10 nm observing that the band gap (E_g) of the material increases as the size of the particle decreases. This property makes it a candidate for opto-electronic applications in many fields such as photography, IR detectors, solar absorbers, light emitting devices and solar cells [4,5]. For a photo-electrochemical solar cell, the ideal band gap (E_g) of semiconductor should be $\sim$1.6 eV. The discrete structure of energy states leads to a discrete absorption spectrum of nanocrystals (NCs). Thus, we can observe an increase in the E_g of semiconductor with a decrease in the particle size [6]. Various nanostructures such as nanorods [7], nanowires, [8], star-shaped particles [9], and dendrites [10] of PbS have been synthesized. The confinement effect appears as a shift in absorption spectra and the absorption to lower wavelengths, which is due to a change in the E_g and control over the assembly or aggregation of particles [11,12].

Thus, intrinsic semiconductor PbS thin films have been studied extensively during the past few decades to explore their size-dependent properties and potential applications in diverse areas. The nature and concentration of dopants are responsible for particular properties and efficiencies of semiconductor NCs. The structural parameters such as crystalline phase, grain size etc. is strongly dependent on the deposition conditions. The key requirements for many of these applications are the doping of PbS with various elements for enhancing and controlling its optical and electrical properties. The IV-VI NCs thin films doped with various metals ions lead to different effects and have attracted major attention as the impurity-atoms doping into the NCs provides sharp atomic levels for capturing exciton electrons and holes from the host semiconductor lattice.

Hence investigation of the role of dopant concentration on structural, optical properties of doped semiconductors NCs is very important from the viewpoints of basic physics as well as applications. Thus, on this frame of reference, in the present work we prepare undoped and Bi^{3+} -doped PbS nanostructured films by means of the green method of chemical bath (CB), in order to investigate their structural, optical properties [13].

Characterization of the thin films was made by Scanning Electron Microscopy (Model JSM-6610LV, JEOL). The elemental composition was obtained by an energy dispersive spectrometer (Oxford Instruments, INCAx-act). Surface roughness of the film was observed using an atomic force microscope (AFM, JSPM5200, JEOL, Japan). The X-ray diffraction patterns of the solid samples were acquired in a D8 Bruker Discover Series 2 diffractometer with Cu K_α radi-

ation of wavelength $\lambda = 1.5408$ Å. Diffraction intensity was measured between 5°, with a 2q step of 0.02° and a counting time of 0.6 s per point. The crystalline phases were identified by means of the JCPDS (Joint Committee of Powder Diffraction Standards) database It was operated at 40 kV and 40 mA. The grain size was determined utilizing the Scherer's formula on XRD patterns. The optical absorption studies were carried out using a UV-VIS-IR spectrophometer (Cary-5000) in the 300-900 nm wavelength range at room temperature, determination of the wavelength of absorption maxima with < 0.5 nm accuracy, to calculate the forbidden band gap energy (E_g) by using the $(\alpha h\nu)^2$ vs. $h\nu$ plot, where α is the optical absorption coefficient and $h\nu$ the photon energy.

2. Chemical reactions and experimental procedure

The reactions for the growth of PbS films doped with Bi^{3+} were determined by employing the cell potential values in basic media already reported [14]. Worth-noting is the formation of the coordination complex $[Pb(NH_3)_4]^{2+}$, which is relevant for the release of Pb^{2+} ions and their slow reaction with S^{2-} ions that, under these conditions, lead to the spontaneous formation to the PbS precipitate in an easily controlled process [15]. (a) The coordination complex $[Pb(NH_3)_4]^{2+}$ is generated indirectly from NH4NO3. (b) The S^{2-} ions are present in the solution and are generated from the thiourea decomposition in alkaline solution. (c) In this work Bi^{3+} ions were chosen as dopant to investigate the optical and structural changes considering that the ionic radius of Bi^{3+} (Pb^{+2} = 0.84 Å, Bi^{3+} = 0.74 Å) is smaller than that of Pb^{2+} ion, allowing its incorporation into the crystal lattice. Therefore a water-soluble salt providing Bi^{3+} ions was chosen. This is a condition for using the green CB technique, which is performed in aqueous solution. The abovementioned steps allow the slow process of deposition onto the substrate surface to take place predominantly over the direct hydrolysis of thiourea in the bulk of the reaction bath [12]:

$$SC(NH_2)_2 + 3OH^- \Leftrightarrow CO_3^{2-} S^2 + 7H^+ \quad (1)$$

$$[Pb(NH_3)_4]^{2+} + S^{2-} \Leftrightarrow PbS + 3NH_4^+$$

$$\Delta G^o = +335.48 \text{ KJ} \quad (2)$$

$$Bi^{3+} + 3e \Leftrightarrow Bi$$

$$\Delta G^o = -89.16 \text{ KJ} \quad (3)$$

$$[Pb(NH_3)_4]^{2+} + S^{2-} + Bi^{3+} \Leftrightarrow PbSBi^{3+} + 4NH_4^+$$

$$\Delta G^o = +273.72 \text{ KJ} \quad (4)$$

From Eq.(4), the free energy change is positive, so this reaction is not spontaneous and favours the incorpora-tion of Bi in an ionic form under the working conditions (pH, temperature, stirring and reagents concentrations).

The preparation of polycrystalline PbS thin films, undoped and doped with $V_{[Bi^{3+}]}$ volume, on glass substrates was carried out by chemical bath (CB) at a temperature of 40 ± 2°C and pH = 11.0. The PbS films with six different levels of doping ($V_{[Bi^{3+}]}$) were obtained by the in situ addition of 5, 10, 15, 20, 25, 30 mLs of $Bi(NO_3)_2$ in the solutions. The quantities of the other reagents and reaction conditions were analogous to those used in previous works [13,15].

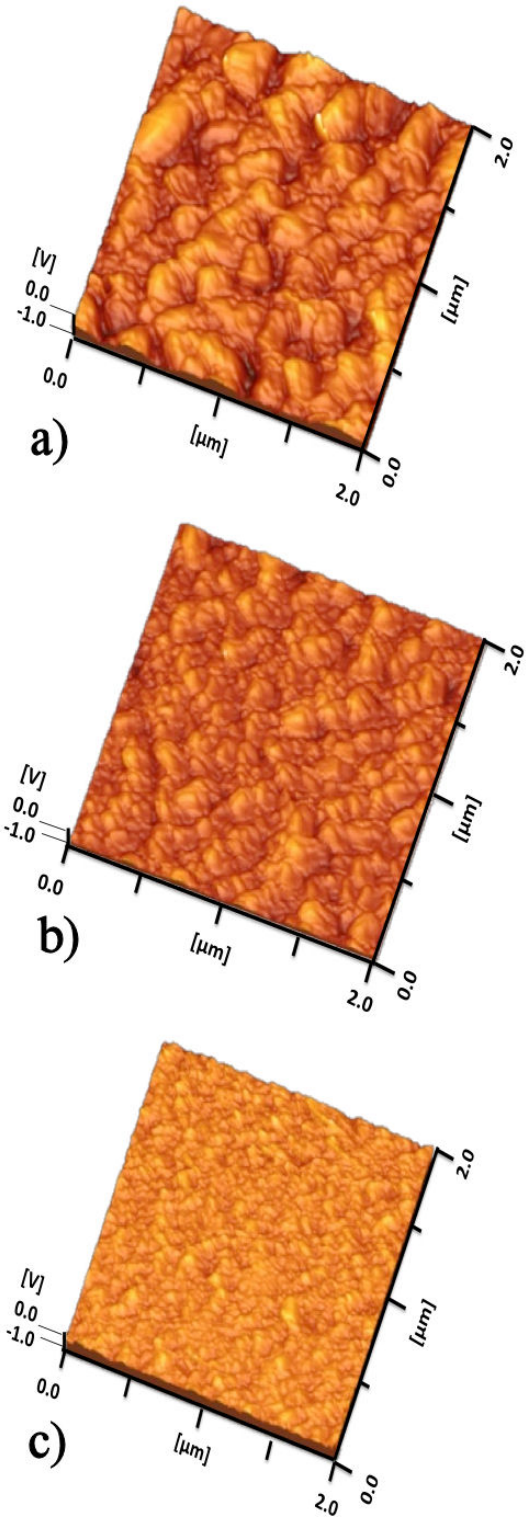

FIGURE 1.

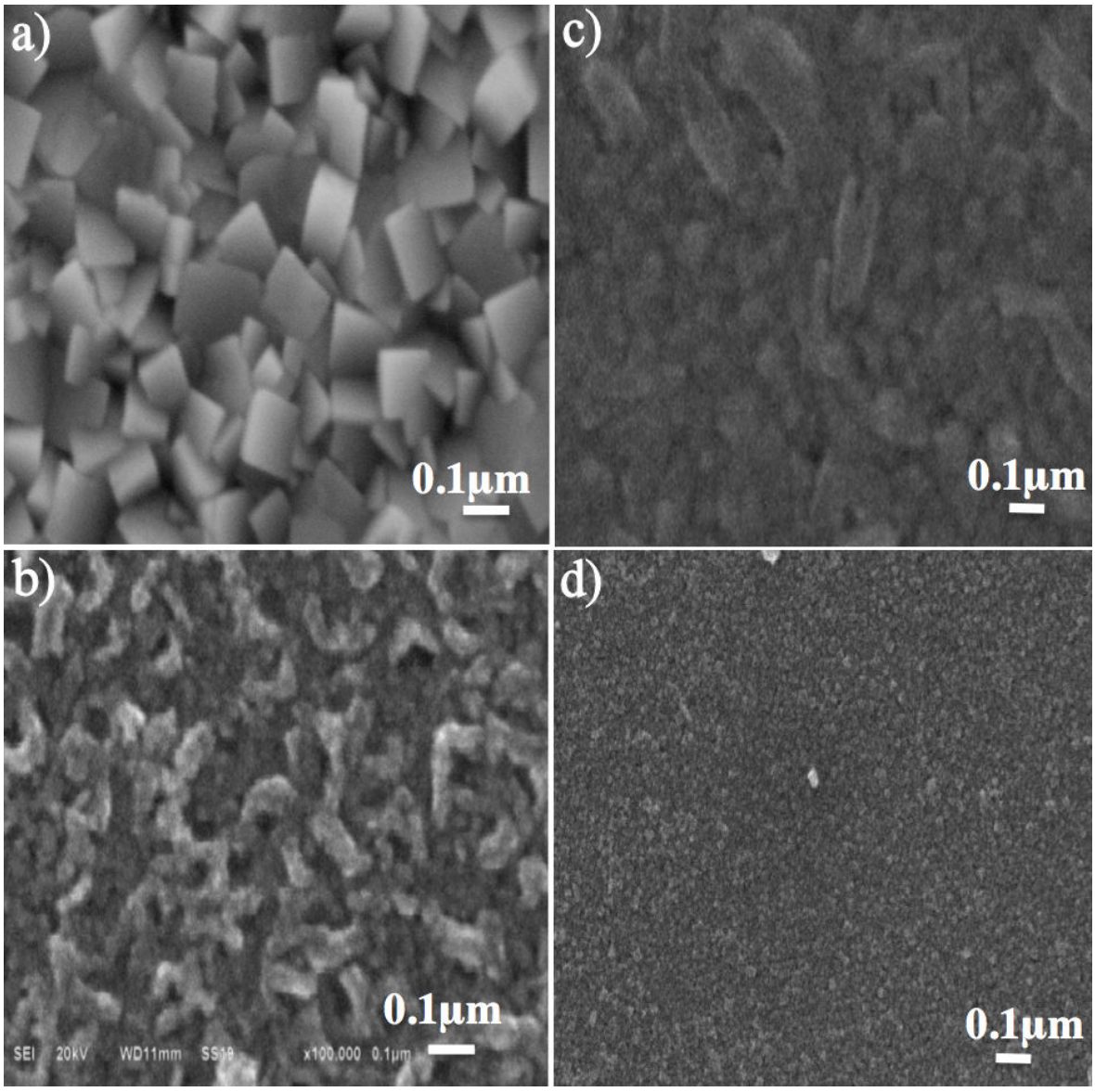

FIGURE 2.

The samples were labelled as PbS0 for the undoped sample and PbSBi5-PbSBi30 for the doped samples. The solutions were thoroughly mixed and the final solution was heated to $40\pm2°$C during 0.5 h, with the substrate remaining inside the solution. The optimal concentration of the doping solution ($V_{[Bi^{3+}]}$) $Bi(NO_3)_2$ (0.031 M) was determined after several trials, until films had attained good adherence. The colour of the chemical bath changed from a colourless and transparent solution to a black and turbid one in less than 15 min.

3. Results and discussion

The 2D and 3D surface images for a 2×2 μm area of the PbS0-PbSBi thin films obtained by AFM are shown in Fig. 1: (a) which corresponds to the PbS0 sample, shows a growth of grains and therefore the particle size distribution is rather broad. Doping with Bi^{+3} for sample PbSBi15 results in a concomitant grain size reduction as can be seen in (b). The surface roughness for the film is very small (6.5 nm) [13]. Figure (c) for the PbSBi30 film shows that the small nanograins, of approximately 40-20 nm in size, are uniformly distributed, forming a smooth homogeneous crystalline film. The effect of increasing the Bi^{+3} dopant on the grain size becomes apparent when comparing the AFM images for samples PbSBi15 and PbSBi30.

The elemental analysis was carried out only for Pb, S and Bi, with the average atomic percentage of Pb and S for undoped and doped samples. The quantitative analysis of the films was carried out by using the energy dispersive spectrometer (EDAX) technique at different points to study the stoichiometry of the films. In Table I are compiled the atomic

concentrations of Pb, S and Bi. It can be appreciated how the concentration of Bi in PbS films increases, reaching a percent value of Bi = 15.22. In this case, when Bi^{3+} enters as substitute of Pb^{2+}, for each Pb^{2+} ions a S^{2-} vacancy would be needed for charge balancing purposes. This could be one of the reasons for the decreasing of S concentration in Table I. Probably for the higher $V_{[Bi^{3+}]}$ values considered here, the material obtained cannot be considered as doped semiconductor; actually, the material can be similar to a solid solution of $Pb_{1-x}Bi_xS$ [13], when Bi^{3+} enters as substitute of Pb^{2+}. The SEM micrographs of PbS0-PbSBi films are shown in Fig. 2, with scale bar: 0.1 μm. In these films: PbS0, PbnSBi05, PbS15Bi, PbS30Bi, the uniform surface morphology can be observed. The SEM micrographs show that the particle grain size decreases with a $V_{[Bi^{3+}]}$ increase concentration. As can be seen, the granules are made of different sizes. The films with doping levels of $V_{[Bi^{3+}]}$ 10, 20, and 25 mLs are not shown. A very adherent film with red metallic aspect was obtained in the doping samples, revealing continuous compact polycrystalline films. The granules are of different sizes; we can conclude that the doping plays a vital rule on the morphological properties of the PbS thin films. As shown in Fig. 2(a), with PbS0 the pyramidal crystallites are uniformly distributed over the surface, yielding thin films with strong compactness. The coalescence of crystallites on thin films surface affirms their privileged orientation along (200) direction. Nevertheless, in Fig. 2(b), (c) and (d), a fat uniform structure can be seen, which in a compact way carpets the substrate surface with PbSBi crystallites of various sizes. The mean size of PbSBi crystallites depends on the doping concentration in the bath solution.

Figure 3 shows the diffractograms for the series of samples. Such X-ray spectra display broad peaks located at the following angular positions: $2\theta = 26.00°$, $30.07°$, $43.10°$, $51.00°$, $53.48°$. However, sample PbSBi15 shows, in addition, a well-defined peak at $2\theta = 28.605°$, corresponding to the (211) XRD plane identical to the mineral bismuthinite (Bi2S3, PDF 17-0320). The first observation about the deposition process developed with $V_{[Bi^{3+}]}$ consists in the change of the induction period of PbSBi precipitation. The induction period is defined as the interval of time elapsed from adding the last reagents to the reaction mixture up to the moment when the precipitate becomes visible. More exactly, it is the time for initiation of the homogeneous chemical precipitation. Comparing the induction period, we a decrease for the preparation performed in the presence of Bi salt solution in the bath can be observed. The increase in nucleation centers density in both cases can explain this behaviour. In our cases it is a fact that the $V_{[Bi^{3+}]}$ accelerates the nucleation process either in the solution or on the substrate. We supposed that, as a result, $V_{[Bi^{3+}]}$ for PbSBi15 sample act as supplementary nucleation centers leading to Bi2S3 impurities. In contrast for other films, Bi2S3 are in-soluble in this conditions of $V_{[Bi^{3+}]}$ excess; thus, the small Bi2S3 particles act as nucleation centers contributing to the decreases of inducting period for homogeneous precipitation. The usual guideline for sequential

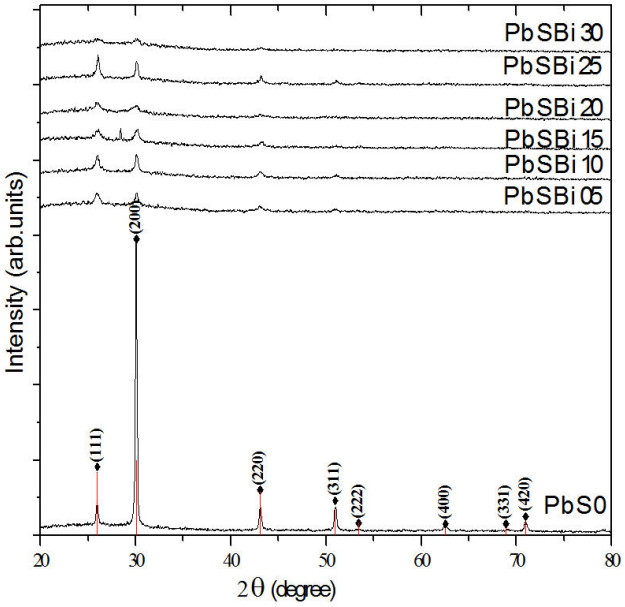

FIGURE 3.

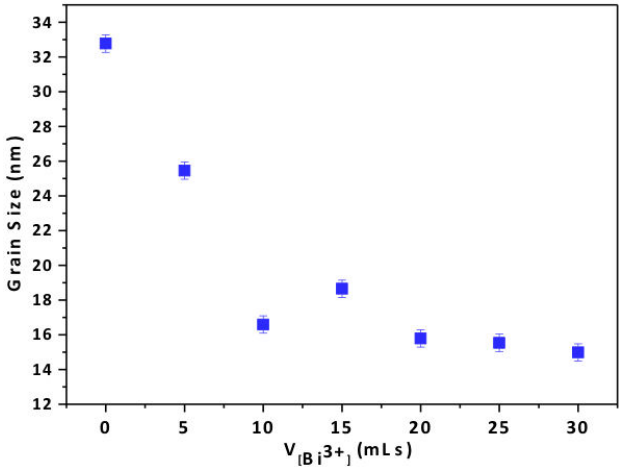

FIGURE 4.

chemical deposition is that the solubility product (ksp) of the base film is lower than that of the subsequent film. In the present case, ksp is 10^{-100} (mol dm^{-3})^5 for Bi_2S_3 and 10^{-28} (mol dm^{-3})^2 for PbS at room temperature. The intensity peak is reached for the PbS0 sample, indicating either the existence of larger num-ber of (200) planes or that the (200) planes have lower number defects [16]. The low intensity (111) and (200) peaks observed in the XRD patterns of the doped PbSBi20-PbSBi30 samples indicates that the films are coarsely fine crystallites or nanocrystalline [17].

The average crystallite size was calculated using the well-known Debye- Scherer's formula:

$$GS = \frac{0.9\lambda}{\beta \cos\theta} \tag{5}$$

Where λ is the wavelength (1.5406 Å), β is the full width at half maximum (in radian) of the peak and θ is Bragg's angle of XRD peak.

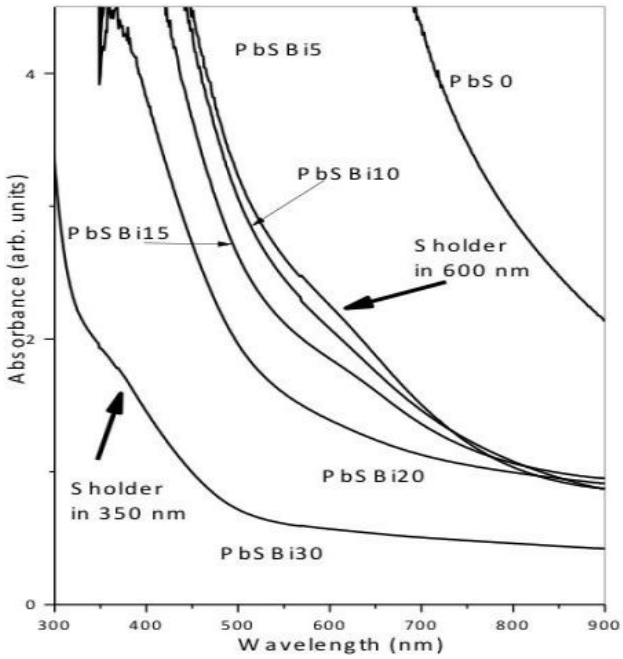

FIGURE 5.

Figure 4 show the average grain size (GS) vs. $V_{[Bi^{3+}]}$ for PbS0-PbSBi samples corresponding to the (220) plane. In this Figure we can be observe that GS reduces, as for PbS0, with GS $\sim$33 nm, and that GS decreases for doped samples in the 25-15 nm range, thus confirming AFM and SEM results. There are two main possible causes for peak broadening. Firstly, an increase in heterogeneity of the films due to the occupation of Bi^{3+} into the host lattice. This phenomenon may be attributed to the doping effect [13,18]. A second cause is a decrease in crystallite size, these effect are associated to the doped PbSBi nanocrystals with $V_{[Bi^{3+}]}$ in the regime where the cluster mechanism is dominating (on the contrary to films grown via ion-ion mechanism, where the crystal size was larger), and consist of PbSBi nanocrystals embedded in an apparent matrix of PbS. The ionic radii data are Pb^{+2} = 0.84 Å, S^{2-} = 1.84 Åand Bi^{3+} = 0.74 Å; therefore for a relative low concentration of Bi^{3+} ions a majority can be located in (i) Pb^{2+} vacancies sites, which otherwise would be empty (ii) in Pb2+ sites, causing the appearance of Pb^{2+} interstitial, and (iii) in interstitial positions. It can be mentioned that as a result, the stable crystal structure of PbS, when Bi^{3+} occupies more and more sites of Pb^{2+} in the host lattice, internal strain would arise, and the crystal structure of PbSBi solid solution becomes unstable. In order to stabilize the crystal structure, the GS is reduced to release the strain. As the Bi^{3+} concentration is increased, the diffraction peaks become broader due to reduction in the GS. At this level of $V_{[Bi^{3+}]}$, the PbSBi can be considered a doped material [13,15]. The effect of the GS decrease by the doping effect has been reported in films of doped PbS [19].

The absorbance spectra vs. λ of various PbSBi samples are depicted in Fig. 5. Typical absorption spectra within 300-900 nm of the PbS0-PbSBi layers as a broad absorbance continuum can be seen rising from a long wavelength tail and peaks at $\sim$350 nm. In these same spectra the fact that the absorbance decreases with the concentration of $V_{[Bi^{3+}]}$ can be observed.The intensity of the absorption increases steadily with the Bi content, and this is similar to most other reports on PbS nanoparticles [21]. The spectra of layers show an absorption onset of 600-700 nm with one salient shoulder around 650 nm. A broad absorbance continuum can be seen rising from a long wavelength tail and shoulder at $\sim$350-600 nm for PbSBi15 and PbSBi30 layers. These exciton peaks were attributed to $1S_e$-$1S_h$ transition [21]. The intensity of the absorption increase steadily with the $V_{[Bi^{3+}]}$, and this is similar to most other reports on PbS nanoparticles [22]. It is well-known that this peak is strongly related to the surface charge separation and polarization effects, and is thus sensitive to changes on the surface molecules [23].

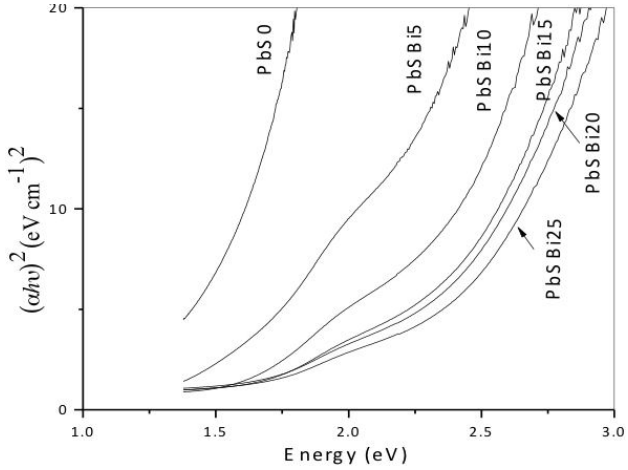

FIGURE 6.

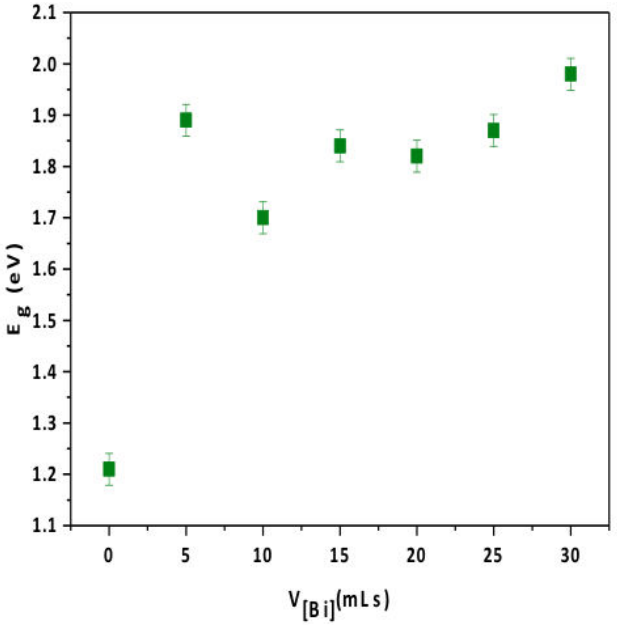

FIGURE 7.

The absorbance spectra of layers show an absorption onset of 500 nm with one salient shoulder around 600 nm. The excitonic absorption peak is reported at ∼625 nm. A broad peak located around ∼655 nm (1.9 eV) appears after PbS nanocrystals produce. The energy transitions in both electron and hole levels of PbS nanocrystals was revealed in four major types, the S_e-S_h, S_e-P_h, P_e-S_h and P_e-P_h transitions [24]. These exciton peaks were attributed to $1S_e$-$1S_h$ transition. The intensity of the absorption increase steadily with the $V_{[Bi^{3+}]}$, and this is similar to most other reports on PbS nanoparticles [22,25].

This is a clear indication of the quantum confinement, since the average GS of the PbSBi nanocrystals is the exciton Bohr radius (18 nm). This may washout the exciton absorption peaks in visible region [26]. The fundamental absorption, which corresponds to the electron excitation from the valence band to the conduction band, can be used to determine the nature and value of the optical band gap (E_g). The procedure consists of plotting α^2 versus $h\gamma$ and extrapolating the linear region of the curve to the energy axis; the intercept being identified as the E_g. Figure 6 shows the plot of $(\alpha h\nu)^2$ versus $h\nu$ for direct transition of PbS0-PbSBi layers. The confinement effect appears as a shift in edge of the absorption spectra and the absorption to lower wavelengths, possibly due to the decrease in GS. It is clearly seen from the optical spectrum an absorption edge shift toward a lower wavelength in doped films. This clearly indicates an increase in the E_g as a result of Bi-doping. Doping of PbS with Bi^{3+} is expected to alter the optical E_g between 0.41 eV (E_g of PbS) and resulting ternary PbSBi alloy [13,19]. However the fundamental E_g (0.41 eV) for PbS0 is not observed in this work. Possibly a solid solution with of PbS with Bi^{3+} is formed, as shown by the DXR results, since a small shift is seen in the diffraction peaks.

The Fig. 7 shows E_g vs. $V_{[Bi^{3+}]}$ plot for the nanoparticle PbS0-PbSBi films. Previously, there were reports about very large Stokes shift in PbS quantum dots (QDs), which were attributed to the presence of localized surface states or trap states [27]. The excitonic peak at 1.73 eV is from ^1S_h to ^1S_e, which is also the optical E_g of this size PbS QDs. Though there has been debate over assignment of the excitonic transition at 1.42 eV, ascribed as ^1P_h to ^1P_e. The excitonic peaks at 1.66 eV, 1.86 eV, 2.157 eV, are due to higher energy transitions from ^1D_h to ^1D_e, ^2S_h to ^2S_h and ^2P_h to ^2P_e, respectively [27]. The emission peak observed at 1.9 eV corresponds to the S_e-S_h transition, which is a lowest energy exciton. The possibility of obtaining optical E_g ranging from 0.41 eV by varying the crystalline diameter of PbS from 12 nm to 2 nm has been reported [21].

A large number of defects like vacancies, interstitials, etc. can act as trap centers and affect the optical absorption. Therefore, an increase in the optical band gap can be primarily associated with defect-induced band tailing due to the creation of localized energy states near the band edges [29]. Therefore, such a strong absorption level has been attributed to the formation of nanoparticles in high concentration of doping Bi^{3+}. The absence of any excitonic absorption structure in absorption spectra may be due to two main reasons: first, the weak exciton binding energy because of strong Coulomb screening in narrow gap semiconductors and second, the existing size distribution of nanocrystals [30].

4. Conclusions

In summary, doped thin films with varying concentration of Bi^{3+} ions were prepared from chemical bath. This is an efficient and green process to introduce Bi^{3+} ions into PbS lattice with, practically, no large damage to the lattice. Preferential orientation along (200) plane for samples indicates that doping favours the three dimensional growth of the films. Improvement in crystallinity accompanied by enhancement in grain size is observed up to optimum concentration. XRD patterns show 2θ = 26.00°, 30.07°, 43.10°, 51.00°, 53.48°, which belong to the ZB phase. Doping improves surface morphology to a great extent. The grain size lies in the interval of 33-15 nm. Optical absorption spectra are quantified for the PbSBi film in which the red-shift of E_g is associated with the decrease of the average GS. Forbidden band gap energy (E_g) shift discloses a shift in the 1.2-2.0 eV range.

1. L.E. Brus, *J. Chem. Phys.* **80** (1984) 4403; N.Choundhury and B.K. Sharma, *Thin Solid Films.* **519** (2011) 2132.
2. Z. Peng, Y. Jiang, Y. Song, C. Wang, and H. Zhang, *Chem. Mater.* **20** (2008) 3153; S. Chandramohan, A. Kanjilal, S. Sarangi, N.S. Majumder, R. Sathamoorthy and T. Som, *Appl. Phys. A* **99** (2010) 837.
3. R. Reisfeld, C.K. Jorgensen (Eds.), vol. 85, Springer, (Berlin, 1996) p. 99. (b) C.Z. Zhang, W.C. Wei and Y.H. Xiao, *Crystal Growth & Design* **7** (2007) 580.
4. P.K. Nair, O. Gomezdaza, M.T.S. Nair, *Adv. Mater. Opt. Electron.* **1** (1992) 139.
5. P.K. Nair, and M.T.S. Nair, *J. Phys. D: Appl. Phys.* **23** (1990) 150; A. Yuchi, H. Wada and G.Nakagawa, *Analy. Sci.* **1** (1985) 19.
6. S.B. Pawar, J.S. Shaikh, R.S. Devan, Y.R. Ma. D. Haranath, P.N. Bhosale and P.S. Patil. *Appl. Surf. Sci.* **258** (2011) 1869.
7. T. Saraidarov, R. Reisfeld, A. Sashchiuk and E. Lifshitz, *Physica E* **37** (2007) 173.
8. D. Yu, W. Zhaoyu Meng, J. Lu and Yitai Quian, *J. Mater. Chem.* **12** (2002) 403.
9. S.-M. Lee, Y.-W. Jun, S.-N. Cho and J. Cheon, *J. Am. Chem. Soc*. **124** (2002) 11244.
10. S. Xiong, B. Xi, D. Xu, C. Wang, X. Feng, H. Zhou, and Y.i Quian. *J. Phys. Chem. 111* (2007) 16761.

11. S. Thangavel, S. Ganesan, K. Saravanan, *Thin Solid Films.* **520** (2012) 5206.
12. R. Gutiérrez Pérez *et al*., *J. Mater. Engin. A* **3** (2013) 1.
13. R. Kumar, P. Kumar, R. Das, and S. Tiwari, *Adv. Phys. Theo. Appl.* **19** (2013) 101.
14. A.J. Bethune, N.A.S Loud, *In Standard Aqueous Potential and Temperature Coefficients at* 25°C, C.C. (1969) Hampel, Skokie, II.
15. O. Portillo Moreno *et al*., *J. Electrochem. Sci. Soc.* **153** (2006) 930
16. O. Zelaya Angel *et al*., *J. Mater Sci.* **1** (2011) 1
17. S. Kaci, A. Keffous, M. Trari, O. Fellahi, H. Menary, A. Manseri, and L. Guerbous, *J. Lumi-nesc.* **130** (2010) 1849.
18. R.K. Joshi, A. Kanjilal, H.K. Shegal, *Appl. Surf. Sci.* **221** (2004) 43.
19. R. Kumar and R. Das, *Inter. Conf. on Adv. in Eng. & Tech*., (ICAET-2014) 7
20. W.P. Lim, H.Y. Low, and W.S. Chin, *J. Phys. Chem. B* **108** (2004) 13093.
21. Y. Wang, A. Suna, W. Mahler and R. Kasowsky, *J. Chem. Phys.* **87** (1987) 7315.
22. P. Prathap, N. Revathi, P.V. Subbaiah and K.T. Ramakrishna, *J. Phys. Condens. Matter.* **20** (2008) 35205.
23. M. Gao, Y. Yang, B. Yang and J. Shen, *J. Chem. Soc. Faraday Trans.* **91** (1995) 4121.
24. J.-H. Chen, C.-G. Chao, J.-C. Ou and T.-F. Liu, *Appl. Surf. Sci.* **601** (2007) 5142.
25. R. Rossetti, R. Hull, J.M. Gibson and L.E. Brush, *J. Chem. Phys.* **83** (1985) 1406.
26. S. Wang and S. Yang, *Langmuir* **16** (2000) 389.
27. J. Zhang and X. Jiang, *Appl. Phys. Lett.* **92** (2008) 14108.
28. W. Bolse, *Mater. Sci. Eng. R* **12** (1994) 53.
29. K. Senthil, D. Mangalaraj, S.K. Narayandas, B. Hong, Y. Roh, C.S. Park and J. Yi, *Semicond. Sci. Technol.* **17** (2002) 97.
30. Chahadin *et al*., *Nanoscale Res, Lett.* **6** (2011) 542.